Computers and Concrete, *Vol. 25, No. 4 (2020) 369-382*
DOI: https://doi.org/10.12989/cac.2020.25.4.369

Finite element modelling of GFRP reinforced concrete beams

Joseph G. Stoner[1a] and Maria Anna Polak[*2]

[1]WSP Canada, 610 Chartwell Road, Suite 300, Oakville, Ontario, L6J 4A5, Canada
[2]Department of Civil and Environmental Engineering, University of Waterloo, 200 University Avenue West, Waterloo, Ontario, N2L 3G1, Canada

(*Received November 8, 2019, Revised March 21, 2020, Accepted March 22, 2020*)

Abstract. This paper presents a discussion of the Finite Element Analysis (FEA) when applied for the analysis of concrete elements reinforced with glass fibre reinforced polymer (GFRP) bars. The purpose of such nonlinear FEA model development is to create a tool that can be used for numerical parametric studies which can be used to extend the existing (and limited) experiment database. The presented research focuses on the numerical analyses of concrete beams reinforced with GFRP longitudinal and shear reinforcements. FEA of concrete members reinforced with linear elastic brittle reinforcements (like GFRP) presents unique challenges when compared to the analysis of members reinforced with plastic (steel) reinforcements, which are discussed in the paper. Specifically, the behaviour and failure of GFRP reinforced members are strongly influenced by the compressive response of concrete and thus modelling of concrete behaviour is essential for proper analysis. FEA was performed using the commercial software ABAQUS. A damaged-plasticity model was utilized to simulate the concrete behaviour. The influence of tension, compression, dilatancy, mesh, and reinforcement modelling was studied to replicate experimental test data of beams previously tested at the University of Waterloo, Canada. Recommendations for the finite element modelling of beams reinforced with GFRP longitudinal and shear reinforcements are offered. The knowledge gained from this research allows for the development of a rational methodology for modelling GFRP reinforced concrete beams, which subsequently can be used for extensive parametric studies and the formation of informed recommendations to design standards.

Keywords: fibre reinforced polymers (FRP); concrete; finite element analysis; ABAQUS; concrete damaged plasticity model; nonlinear finite element analysis

1. Introduction

The application of fibre reinforced polymer (FRP) bars as internal reinforcement for concrete structures has increased in recent years as an alternative to steel products due to the material's high tensile strength, light weight, and inability to corrode electrochemically. The utilization of this new type of reinforcement is driven primarily by FRP's durability in corrosive environments. Steel reinforcement is susceptible to corrosion under typical environmental conditions, resulting in delamination, spalling, overall deterioration of the concrete, and reduction of the area of reinforcement available to carry tensile stresses. FRP has been used successfully as internal reinforcement for concrete structures including bridge decks, concrete barrier walls, parking garage slabs, and containment structures that house corrosive materials.

The behaviour of concrete members reinforced with GFRP reinforcements is different than the behaviour of traditional concrete members with steel reinforcements. Compared to steel, GFRP is a strong, but less stiff, brittle material that is linear elastic until failure. Reinforced concrete members with GFRP rely on concrete ductility in compression to achieve the required structural deformability. Experimental test programs are essential to gain an understanding of the behaviour and failure modes of such concrete members. Laboratory testing, however, is often expensive, time consuming, and may be impractical in studying the effects of several parameters on the behaviour of structural members. The use of analytical methods, such as finite element analysis (FEA), in combination with experimental testing, allows one to gain an understanding of the structure's behaviour. This also enables future experiments to be designed more rationally, thereby producing more meaningful results that contribute to the progression of the field.

The primary challenge with the FEA of concrete with linear elastic, brittle reinforcements is that the results are dependent on the proper modelling of concrete; much more than such analyses performed for concrete with yielding steel reinforcements. As the reinforcement does not yield, the member failures are driven by either concrete cracking or concrete crushing; therefore, the proper compressive tensile and compressive modelling of the concrete is essential to capture these failure modes. Modelling of GFRP is done using simple linear elastic brittle models. However, GFRP does influence concrete confinement and this needs to be included in the materials modelling of concrete.

FEA of fiber reinforced polymer (FRP) reinforced concrete (RC) have been done by several researchers. Ferreira *et al*. (2001) performed finite element analyses of

*Corresponding author, Professor
E-mail: polak@uwaterloo.ca
[a]M.A.Sc.
E-mail: joseph.g.stoner@gmail.com

Copyright © 2020 Techno-Press, Ltd.

ISSN: 1598-8198 (Print), 1598-818X (Online)

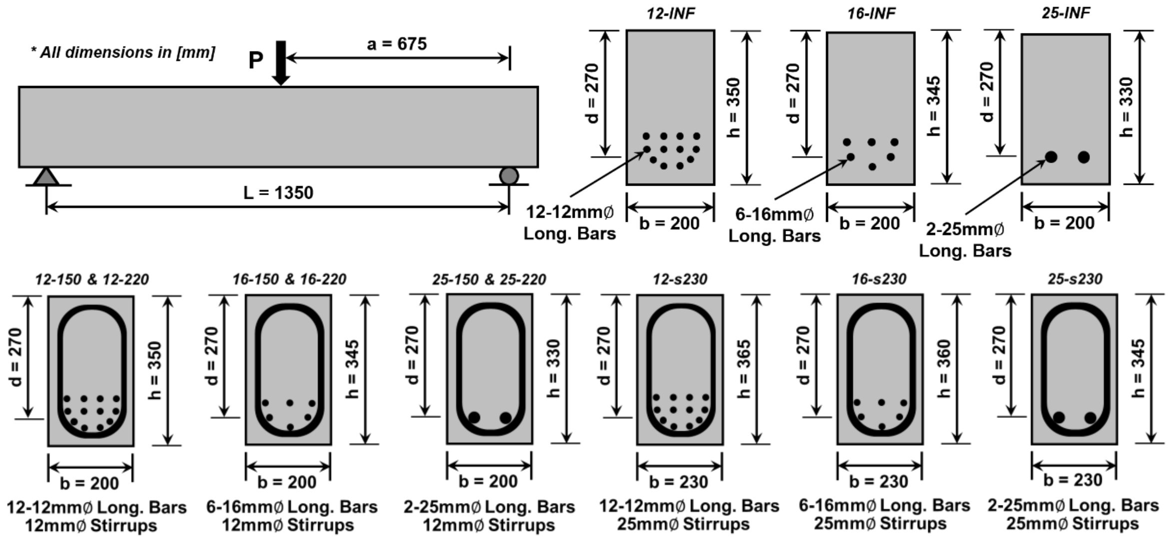

Fig. 1 Experimental test setup and beam cross-sections

concrete beams reinforced with GFRP bars, utilizing a smeared crack approach to model the concrete in tension and elastic-brittle layers of equivalent thickness to model the GFRP bars. Nour *et al*. (2007) used ABAQUS finite element analysis software to analyse slender rectangular beams reinforced with GFRP longitudinal bars and steel stirrups; two-noded truss elements embedded into solid concrete elements were used to model the reinforcement. Rafi *et al*. (2007) modeled concrete beams reinforced with CFRP using the finite element analysis software DIANA, and modelled the behaviour of cracked concrete based on fracture energy. Adam *et al*. (2015) used FEA program ANSYS to investigate behaviour of concrete beams with GFRP bars manufactured by the authors as part of their testing and analysis program. Deep GFRP RC beams were studied by Mohammed *et al.* (2017), where they investigated the relationship between nonlinear FEA and Strut and Tie (ST) modelling of deep concrete beams with GFRP reinforcements. They used the VecTor 2 software and 2-D FEA model. Kaya and Yaman (2018) used ABAQUS to investigate anchorage problem of GFRP strengthening plates in concrete T-Beams.

In most recent studies, several projects were done on the use of FEA as the tool for investigating design parameters and their effect on structural performance of FRP reinforced structural concrete. Yumaa and Yousif (2019) modelled size effect in FRP reinforced concrete beams using the commercial software Abaqus and concrete damages plasticity (CDP) model. They calibrated the model based on experimental test results, showed effect of several modelling parameters on FEA predictions and compared the result to the current codes. Arafa *et al*. 2019 modeled GFRP reinforced concrete walls using a 2-D FEA. After calibrating the model, they performed parametric studies on axial load ratio and vertical web reinforcement effect on lateral load resisting strength of squat walls. Saleh *et al.* (2019) investigated numerically behaviour of GFRP reinforced beams under low velocity impact loads.

This paper presents the numerical analyses of concrete beams reinforced with internal GFRP bars using the commercial finite element analysis software ABAQUS (version 6.12). The purpose of such nonlinear FEA model development is to create a tool that can be used for numerical parametric studies, extending the existing (and limited) experimental database. Beams with and without shear reinforcement are modelled and studied. It should be emphasized that modelling the behaviour and failure of beams with GFRP stirrups presents a special challenge of addressing confinement of concrete. First, an overview of the material model for concrete used in ABAQUS, the Concrete Damaged Plasticity (CDP) model, is presented. Second, the influence that various material parameters and mesh refinement have on the member responses, reinforcement strains, and crack propagation in the concrete beams is presented. Finally, the results of the proposed FEA models are compared with other strength prediction. The calibrated nonlinear FEA can be used in future studies of GFRP reinforced members and help in creating modern and rational design methods for such members.

2. Experimental test program

To calibrate the finite element models presented in this paper, the beam tests performed by Krall (2014) at the University of Waterloo were used. This experimental investigation studied the influence of the flexural and shear reinforcement arrangement on the shear strength and failure mode of concrete members reinforced with GFRP bars. Three-point bending tests were performed on simply-supported concrete beams. Fig. 1 depicts the typical test setup and the cross-sections for each beam.

The cross-sectional dimensions and reinforcement arrangements for the beams are shown in Fig. 1. Nine beams had a constant width of b=200 mm and three beams had a width of b=230 mm. All beams had a constant span of L=1350 mm. The beam height, h, was selected for each beam to maintain a constant shear span to effective depth (a/d) ratio of 2.5 for all beams. All beams were designed to be semi-deep members with a unique longitudinal bar

Table 1 Beams' details

Beam	Cross-Section Dimensions				Long. Reinforcement Layout			Shear Reinforcement	
	b (mm)	h (mm)	d (mm)	a/d	d_b (mm)	No. of Bars	ρ_l (%)	d_b (mm)	Spacing (mm)
BM 12-INF	200	350	270	2.5	12	12	2.51	-	-
BM 16-INF	200	345	270	2.5	16	6	2.23	-	-
BM 25-INF	200	330	270	2.5	25	2	1.82	-	-
BM 12-150	200	350	270	2.5	12	12	2.51	12	150
BM 16-150	200	345	270	2.5	16	6	2.23	12	150
BM 25-150	200	330	270	2.5	25	2	1.82	12	150
BM 12-220	200	350	270	2.5	12	12	2.51	12	220
BM 16-220	200	345	270	2.5	16	6	2.23	12	220
BM 25-220	200	330	270	2.5	25	2	1.82	12	220
BM 12-s230	230	365	270	2.5	12	12	2.18	20	230
BM 16-s230	230	360	270	2.5	16	6	1.94	20	230
BM 25-s230	230	345	270	2.5	25	2	1.58	20	230

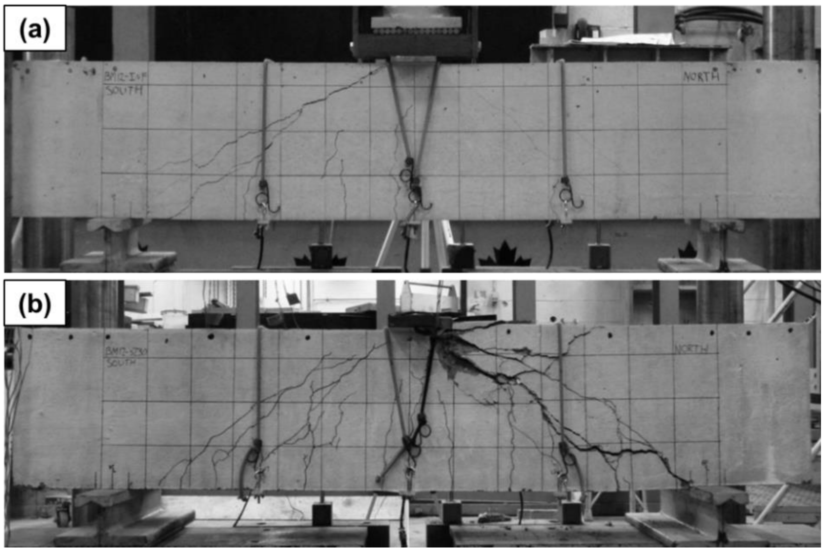

Fig. 2 Typical failure modes (a) Beams with No Stirrups: BM 12-INF, (b) Beams with stirrups: BM 12-s230 (image courtesy of Krall 2014)

diameter and arrangement. Three beams without stirrups and nine beams with stirrups were tested. Table 1 summarizes the beam dimensions and reinforcement layout details, where d_b and ρ_l are the bar diameter and reinforcement ratio, respectively.

Fig. 2(a) and 2(b) depict the typical failure modes for beams without stirrups and for beams with stirrups, respectively. The three beams with no stirrups experienced shear-tension failures. The beams with stirrups experienced higher failure loads than beams without stirrups and failed by crushing of the compression strut. Strain gauges were used to record the axial strains in the longitudinal and transverse bars and linear variable displacement transformers (LVDTs) were used to measure beam deflections during testing.

3. Overview of finite element models

The commercial finite element analysis software ABAQUS/Standard was used for all simulations presented in this paper (DSS, 2012). Three-dimensional analyses were performed. Due to the symmetry of the beam geometries and applied loading, only one-half of each beam was analyzed to reduce the computational demand required. Displacement-controlled loading was used in order to study the post-peak deflection response for each beam. Fig. 3 presents the displacement (U) and rotation (UR) boundary and loading conditions that were applied to each beam to simulate the simply-supported condition.

Each beam was loaded by imposing a downwards displacement to all nodes at the beam midspan. To calculate the total applied load at a given deflection, the vertical reaction forces at the support nodes were summed and multiplied by 2 (three-point bending).

ABAQUS/Standard uses the Newton's iterative method to solve nonlinear equilibrium equations. The selection of the maximum increment size is important for accuracy. To establish an effective maximum displacement increment, ABAQUS/Standard was used to model a concrete cube of unit size (1×1×1) under uniaxial compression. This simple model was analyzed using various values for the maximum

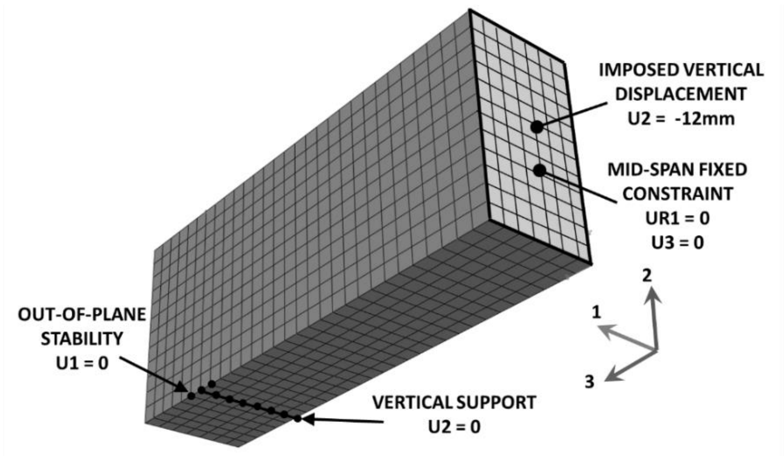

Fig. 3 Boundary conditions and loading model

Table 2 Material properties used in ABAQUS models

Beam	Concrete		GFRP Longitudinal Bars				GFRP Shear (bent) Bars				
	f_c' (MPa)	f_t' (MPa)	d_b (mm)	A_{frp} (mm^2)	f_{frp} (MPa)	E_{frp} (GPa)	d_b (mm)	A_{frp} (mm^2)	f_{frp} (MPa)	$f_{frp,bend}$ (MPa)	E_{frp} (GPa)
BM 12-INF	54.0	2.42	12	113	1000	60	12	113	1000	700	50
BM 16-INF	53.4	2.41	16	201	1000	64	12	113	1000	700	50
BM 25-INF	52.0	2.38	25	491	1000	60	12	113	1000	700	50
BM 12-150	56.5	2.48	12	113	1000	60	12	113	1000	700	50
BM 16-150	56.5	2.48	16	201	1000	64	12	113	1000	700	50
BM 25-150	56.5	2.48	25	491	1000	60	12	113	1000	700	50
BM 12-220	56.5	2.48	12	113	1000	60	12	113	1000	700	50
BM 16-220	56.5	2.48	16	201	1000	64	12	113	1000	700	50
BM 25-220	56.5	2.48	25	491	1000	60	12	113	1000	700	50
BM 12-s230	56.5	2.48	12	113	1000	60	20	314	900	550	50
BM 16-s230	56.5	2.48	16	201	1000	64	20	314	900	550	50
BM 25-s230	56.5	2.48	25	491	1000	60	20	314	900	550	50

increment. It was concluded that increment sizes larger than 0.01 failed to accurately capture the non-linear regions of concrete under uniaxial compression. Therefore, considering both accuracy and computational efficiency, a maximum displacement increment of 0.01 was used for all models.

Table 2 presents the material properties used for the ABAQUS modelling of each beam, including the concrete compressive strength f_c', concrete tensile strength f_t', GFRP tensile strength f_{frp}, GFRP tensile strength at bends $f_{frp,bend}$, and GFRP tensile modulus of elasticity E_{frp}. The cracking stress, f_{cr}, for concrete in direct tension was used to predict the concrete's tensile strength, where $f_{cr} = 0.33\sqrt{f_c'}$ (MPa). Table 2 also presents the properties of the reinforcing bars, including the bar diameters and cross-sectional areas d_b and A_{frp}, respectively.

4. Concrete modelling

4.1 Concrete damaged plasticity model

Concrete Damaged Plasticity Model (CDPM), available in ABAQUS, was used for the presented computations. The CDPM, although more computationally expensive than other concrete models in ABAQUS, incorporates assumptions and features that are more representative of concrete and increases the model's versatility under various loading conditions.

The Concrete Damaged Plasticity Model uses the yield condition proposed by Lubliner *et al.* (1989) with the modifications proposed by Lee and Fenves (1998), and is defined in Eqs. (1a)-(1d).

$$F = \frac{1}{1-\propto}\left[\bar{q} - 3\propto\bar{p} + \beta(\tilde{\varepsilon}^{pl})\langle\hat{\bar{\sigma}}_{max}\rangle - \gamma\langle-\hat{\bar{\sigma}}_{max}\rangle\right] - \bar{\sigma}_c\left(\tilde{\varepsilon}_c^{pl}\right) = 0 \tag{1a}$$

$$\alpha = \frac{(\sigma_{bo}/\sigma_{co})-1}{2(\sigma_{bo}/\sigma_{co})-1} \tag{1b}$$

$$\beta = \frac{\bar{\sigma}_c\left(\tilde{\varepsilon}_c^{pl}\right)}{\bar{\sigma}_t\left(\tilde{\varepsilon}_t^{pl}\right)}(1-\alpha) - (1+\alpha) \tag{1c}$$

$$\gamma = \frac{3(1-K_c)}{2K_c-1} \tag{1d}$$

The terms α and γ represent dimensionless material constants. The term α is a function of the ratio of the biaxial compressive strength to the uniaxial compressive strength, σ_{bo} and σ_{co}, respectively. Kupfer *et al.* (1969) showed that specimens subjected to equal biaxial

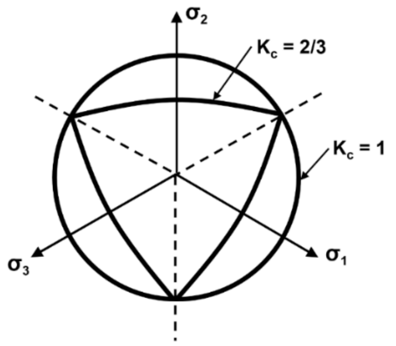

Fig. 4 Failure surface in the deviatoric plane (adapted from DSS 2012)

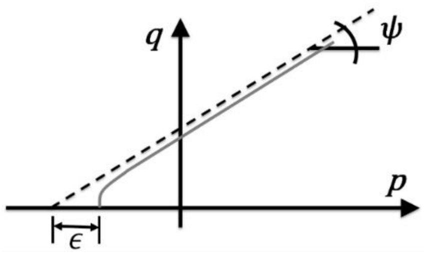

Fig. 5 Plastic potential function in the meridional plane (modified from DSS 2012)

compression yielded a 16% higher strength than uniaxially loaded specimens. Lubliner *et al*. (1989) showed that experimental values of σ_{bo}/σ_{co} range from 1.10 to 1.16. Therefore, the default value of σ_{bo}/σ_{co}=1.16 was used for all models.

The term β is a function of the effective compressive cohesion stress and the effective tensile cohesion stress, $\bar{\sigma}_c(\tilde{\varepsilon}_c^{pl})$ and $\bar{\sigma}_t(\tilde{\varepsilon}_t^{pl})$, respectively. The term γ only appears under states of triaxial compression and is a function of the parameter K_c. K_c is used to control the shape of the failure surface in the deviatoric plane, and is the ratio of the second stress invariant on the tensile meridian to the second stress invariant on the compression meridian. When K_c takes a value of 1.0, the failure surface projection on the deviatoric plane becomes a circle, corresponding to the original Drucker-Prager hypothesis as shown in Fig. 4. Yu *et al*. (2010) recommends the use of a non-circular failure surface to account for the influence of the third deviatoric stress invariant. Furthermore, the original model proposed by Lubliner *et al*. (1989) recommends a range of 0.64 to 0.80 for K_c. Therefore, the ABAQUS default value of K_c=2/3 was used for all models.

The CDPM utilizes a non-associated plastic potential flow rule. The plastic potential flow function, G, used by the CDPM is a hyperbolic Drucker-Prager function and is expressed in the meridional plane using Eq. (2) as shown in Fig. 5.

$$G = \sqrt{\epsilon \sigma_{to} tan\psi + \bar{q}^2} - \bar{p} tan\psi \qquad (2)$$

In Eq. (2), ϵ is a parameter referred to as the plastic potential eccentricity, σ_{to} is the tensile strength of the concrete, and ψ is the dilation angle of the concrete. The eccentricity is a small positive value which defines the rate

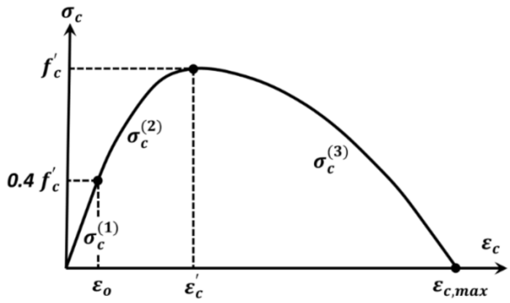

Fig. 6 Concrete uniaxial compression model

that the plastic potential function approaches the classic linear Drucker-Prager function (dashed line shown in Fig. 5). The default value of ϵ=0.1 was used for all models.

The dilation angle of concrete, ψ, is a material parameter that represents the inclination of the plastic potential flow function within the meridional plane as shown in Fig. 5. Typical values for the dilation angle for normal grade concrete range from 30° to 40° as presented in the literature. It has been shown that smaller angles will produce more brittle responses, whereas larger angles will produce responses with higher ductility and larger peak loads (Malm 2006, Janowiak and Lodygowski 2005). The influence of the dilation angle on the beam responses was studied by the authors and is presented in a later section.

4.2 Concrete uniaxial compression model

The modified Hognestad Parabola constitutive equations were used to model the concrete uniaxial compressive behaviour as shown in Fig. 6.

Eqs. (3a)-(3c) represent the three regions of this response, where $\varepsilon_c' = 2f_c'/E_{ct}$, $E_{co} = 5000\sqrt{f_c'}$, and $E_{ct} = 5500\sqrt{f_c'}$ (all in SI units).

$$\sigma_c^{(1)} = E_{co}\varepsilon_c \qquad for\ \sigma_c \le 0.4\,f_c' \qquad (3a)$$

$$\sigma_c^{(2)} = f_c'\left[2\left(\frac{\varepsilon_c}{\varepsilon_c'}\right) - \left(\frac{\varepsilon_c}{\varepsilon_c'}\right)^2\right] \quad for\ \frac{\varepsilon_c}{\varepsilon_c'} \le 1.0 \qquad (3b)$$

$$\sigma_c^{(3)} = f_c'\left[1 - \left(\frac{\frac{\varepsilon_c}{\varepsilon_c'} - 1}{2}\right)^2\right] \quad for\ \frac{\varepsilon_c}{\varepsilon_c'} > 1.0 \qquad (3c)$$

In Eq. (3), ε_c is the concrete compressive strain, ε_c' is the concrete strain at peak stress, $\varepsilon_{c,max}$ is the concrete strain corresponding to a complete loss of strength, f_c' is the concrete compressive strength [MPa], E_{co} is the initial undamaged modulus of elasticity [MPa], and E_{ct} is the initial tangential modulus of elasticity [MPa]. This compressive response assumes the concrete is linear-elastic up to a stress of $\sigma_c = 0.4f_c'$. Beyond this point, the concrete becomes plastic and undergoes strain-hardening up to the maximum compressive strength $\sigma_c = f_c'$, followed by a strain-softening post-peak response. The post-peak response of concrete in compression plays an important role when modelling cases where confinement of concrete influences the member response, therefore the effect of $\varepsilon_{c,max}$ is studied in this paper.

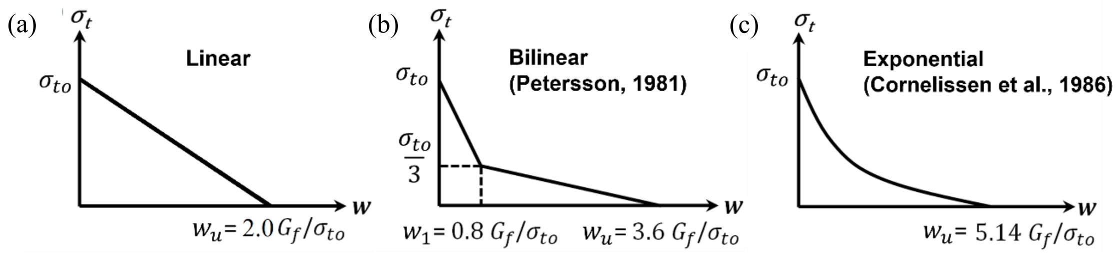

Fig. 7 Post-cracking stress-displacement curves

Table 3 Comparison of fracture energy models

Beam	f_c' (MPa)	f_{ck} (MPa)	f_{cm} (MPa)	G_f (N/m) Model Code (1990)	Trunk and Wittman (1998)	fib Bulletin 42 (2008)	Model Code (2010)
BM 12-INF	54.0	52.4	60.4	91.3	165.7	157.1	152.7
BM 16-INF	53.4	51.8	59.8	90.7	165.7	156.8	152.5
BM 25-INF	52.0	50.4	58.4	89.2	165.7	156.3	151.8
All Beams with stirrups	56.5	54.9	62.9	94.0	165.7	158.0	153.8

4.3 Concrete uniaxial tension model

The tensile behaviour of the concrete was modelled as linear-elastic prior to cracking. The tensile strength of the concrete was taken as $\sigma_{to} = 0.33\sqrt{f_c'}$ [MPa]. A fracture mechanics approach was used to model the post-cracking tensile behaviour. The post-cracking tensile stress (σ_t) was defined as a function of the crack-opening-displacement, w. Fig. 7 depicts various stress-displacement curves that have been proposed in the literature.

The area under each of the curves shown in Fig. 7 represents the concrete's fracture energy, G_f, as was first proposed by Hillerborg *et al*. (1976). Fracture energy is a material property used in brittle fracture mechanics to define the energy required to open a crack of unit area. Various models, with significant scatter, have been proposed to estimate the fracture energy of concrete. Eqs. (4a)-(4d) present four models that were considered: (1) Model Code 1990; (2) Trunk and Wittman (1998); (3) fib Bulletin 42 (2008); and (4) Model Code 2010.

$$G_f = G_{Fo}\left(\frac{f_{cm}}{f_{cmo}}\right)^{0.7} \tag{4a}$$

$$G_f = a d_{\max}^n \ ; \ a = 80.6, n = 0.32 \tag{4b}$$

$$G_f = G_{Fo}\left(1 - \frac{0.77 f_{cmo}}{f_{cm}}\right) \tag{4c}$$

$$G_f = 73(f_{cm})^{0.18} \tag{4d}$$

In Eqs. (4a)-(4d), f_{cmo}=10 MPa and $f_{cm} = f_{ck} + 8$ MPa. The characteristic compressive strength, f_{ck}, was calculated as $f_{ck} = f_c' - 1.6$ MPa as proposed by Reineck *et al*. (2003). In Eq. (4a), G_{Fo} is a function of the maximum aggregate size, d_{max}. For the beams presented in this paper, the maximum aggregate size was 9.5 mm, thus a value of $G_{Fo} = 26$ Nm/m^2 was considered. For Eq. (4c), G_{Fo} is a constant, 0.18 N/mm. Table 3 presents the concrete fracture energy for all beams as predicted using the four models considered.

Table 3 shows that the fracture energy predictions ranged from approximately 90 N/m to 165 N/m. While the magnitude of G_f controls the ability of the concrete to carry tensile stresses after cracking, the shape of the stress-displacement curve controls the rate at which the concrete loses its ability to carry tensile stresses after cracking. Therefore, the influences of various fracture energy values and stress-displacement curve shapes were studied and are presented in a later section.

To account for the tensile carrying ability of concrete between cracks, the tensile strains are defined by dividing the crack-opening-displacement, w, by the characteristic length of the element, l_c; where l_c is the cubic root of the element's volume ($l_c = \sqrt[3]{V}$). For the bilinear post-cracking tension model (Fig. 7), for example, the peak tensile stress σ_{to} corresponds to the cracking strain, ε_{cr}. The tensile strain at the transition point of the two linear segments can therefore be represented as $\varepsilon_1 = \varepsilon_{cr} + w_1/l_c$, and the ultimate tensile strain can be represented as $\varepsilon_u = \varepsilon_{cr} + w_u/l_c$. Therefore, the element size influences the post-cracking stress-strain behaviour, which will influence the amount of tension stiffening and deflection that each beam will experience. The influence of the element sizes used in the analyses on the beam responses is discussed in this paper.

4.4 Concrete damage modelling

The CDPM allows the user to specify scalar isotropic damage parameters for both compression and tension to consider the weakened, or damaged, modulus of elasticity of concrete as a result of plastic deformations. The degraded elastic stiffness for tension and compression are characterized by damage parameters d_t and d_c, respectively (Fig. 8). These parameters take values ranging from zero to one, with a value of zero corresponding to the undamaged material and a value of one corresponding to a complete loss of strength. To prevent convergence issues, damage parameters were limited to a maximum value of 0.90, representing 90% reduction of the elastic stiffness.

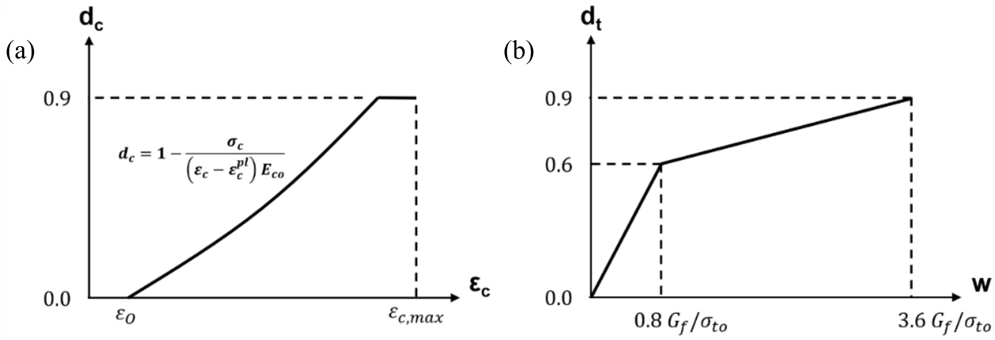

Fig. 8 (a) Compression damage parameters; (b) Tension damage parameters

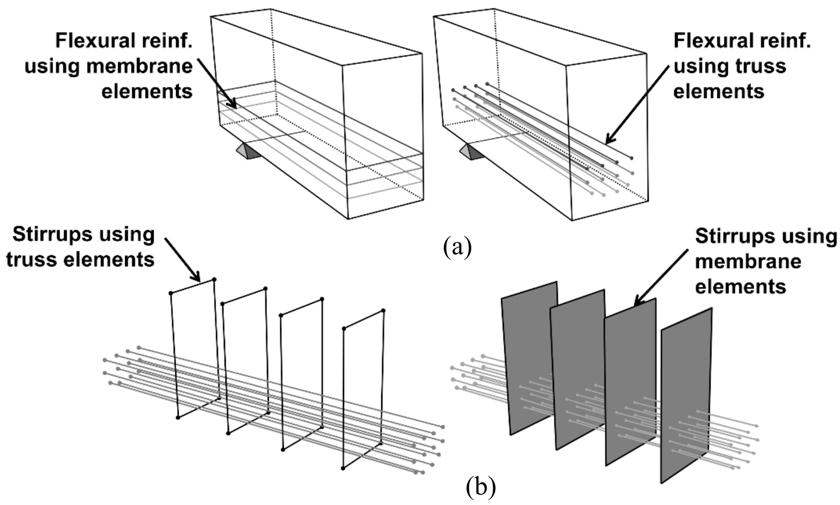

Fig. 9 Reinforcement modelling: (a) Longitudinal reinforcement, (b) Transverse reinforcement

As shown in Fig. 8(a), compression damage was initiated at the onset of inelastic strains (ε_O), and was defined as a function of the concrete plastic strains, ε_c^{pl}. To approximate the plastic strain associated with a given total compressive strain ε_c, the model proposed by Polling (2001) was implemented (Eq. (5)).

$$\varepsilon_c^{pl} = b_c \varepsilon_c^{in} \tag{5a}$$

$$\varepsilon_c^{in} = \varepsilon_c - \frac{\sigma_c}{E_{co}} \tag{5b}$$

where ε_c^{in} is the inelastic compressive strain and b_c=0.7. Fig. 8(b) shows that the tension damage parameters were defined as a function of the crack-opening-displacement w. Tension damage is initiated at cracking, and follows a bilinear relationship. For both compression and tension the reduced stiffness if calculated as: $E_{damaged} = (1 - d_{(c\ or\ t)})E_{c0}$.

4.5 GFRP reinforcement modelling

All GFRP reinforcing bars used in the beam specimens were ComBAR as provided by Schoeck Canada with material properties as defined in Table 2. The GFRP bars were modelled as linear elastic up to the ultimate tensile stress f_{frp}, with a tensile stiffness E_{frp}.

Two methods of modelling the reinforcing bar elements were studied: (1) Discrete truss elements; and (2) Smeared reinforced membrane elements. The first method involved modelling each bar with 2-noded truss elements that transmit axial loading only.

The second approach involved modelling the reinforcement as reinforced membrane sections which are treated as smeared layers with an equivalent thickness equal to $t_{eq} = A_{bar}/S$. The user specifies the cross-sectional area (A_{bar}), spacing (S), material, and orientation of the reinforcing bars within the membrane. 4-noded quadrilateral membrane elements were used to mesh each membrane section. Fig. 9 depicts the two reinforcement modelling methods considered. For both methods, the reinforcement was incorporated into the model using the “Embedded Region” constraint, which constrains the translational degrees of freedom of the reinforcement to the values corresponding to the concrete “host” elements.

5. Calibration and results

5.1 Tension modelling

The influence of the concrete’s fracture energy, G_f, and the shape of the post-cracking stress-displacement relationship on each beam’s response is investigated first. Fig. 10(a) shows the applied load vs. midspan deflection

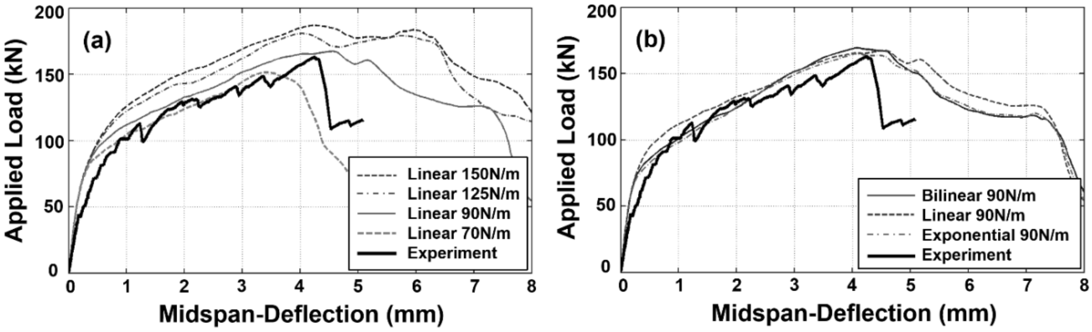

Fig. 10 Influence of tension model on a beam without shear reinforcement, Beam 12-INF

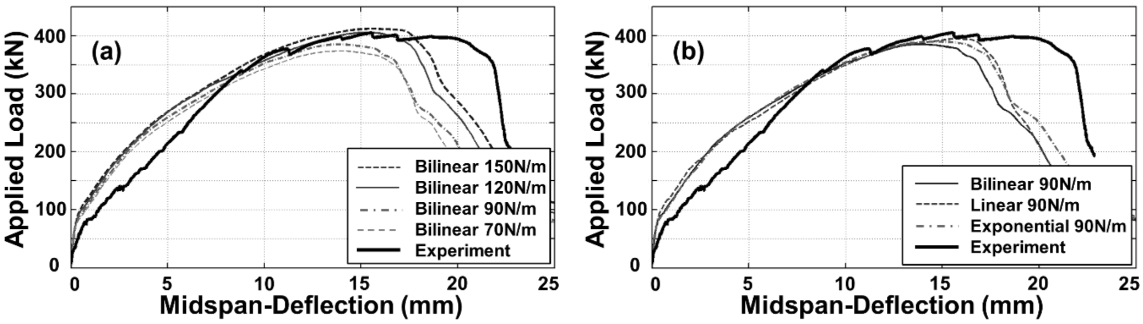

Fig. 11 Influence of tension model on a beam with shear reinforcement, Beam BM 12-150

response for Beam BM12-INF using fracture energy values ranging from 70 N/m to 150 N/m, and compares the results to the experiment measurements. A linear stress-displacement tension model was used for all cases as shown in refer to Fig. 7(a).

For the beams without shear reinforcement (like BM 12-INF) where the failure was controlled by cracking of concrete, the value of fracture energy adopted had a significant influence. Lower fracture energies, 70 N/m specifically, caused the beam to experience a more sudden and brittle failure, whereas higher fracture energy values led to larger deflections and higher failure loads. Similarly, Fig. 11(a) shows the responses for beam BM 12-150 which represents the typical response of beams with shear reinforcement. Comparing Fig. 10(a) and Fig. 11(a), the responses are much less dependent on fracture energy modelling than the responses of beams without shear reinforcement; this is to be expected as the beams with shear reinforcement failed by crushing of concrete, therefore compression modelling is more critical in these cases.

Fig. 10(b) and Fig. 11(b) show the influence of the shape of the post-cracking tensile stress-displacement relationship on the beam response with a constant fracture energy of 90 N/m. Three relationships were considered as introduced in Fig. 7: linear, bilinear, and exponential. All three models produced similar failure loads. The difference between each model is observed in the deflection response of beams without stirrups in the post-cracking region prior to the peak load. The linear relationship produced a stiffer response after cracking than the other models; this is to be expected as the linear model implements a slower rate of tensile carrying capacity decay than the other models. The bilinear and exponential tension models yielded identical results and were better able to represent the concrete's post-cracking stiffness than the linear relationship. For beams with shear reinforcement the shape of the post-cracking tensile stress-displacement relationship had little influence on the predicted response as sown in Fig. 11(b). It was concluded that the bilinear stress-displacement response proposed by Petersson (1981) with a fracture energy of G_f=90 N/m produced model responses with the strongest agreement with the experimental data and was used for all beams.

5.2 Compression modelling

The effective modelling of concrete in compression was found to be essential for capturing the behaviour of beams reinforced with GFRP. This was particularly important for beams with GFRP stirrups, as such reinforcements do not yield at failure and the members with shear reinforcement failed due to compression crushing. Modelling of compression includes two parameters, which need to be investigated together, namely the maximum strain $\varepsilon_{c\,max}$ and the dilation angle ψ (see Eqs. (2) and (3), and Figs. 5 and 6).

First the behaviour of beams without shear reinforcement is investigated. Based on Eq. (3) and an average value of $f_c' = 54\,\text{MPa}$, the value for $\varepsilon_{c,max}$ is equal to 0.008. Fig. 12(a) shows the influence of various dilation angles, ranging from 20° to 50°, on the load-deflection response for BM 12-INF (with $\varepsilon_{c,max} = 0.008$). Fig. 12(b) shows the response of BM 12-INF for various $\varepsilon_{c,max}$ values (with dilation angle ψ =30^0).

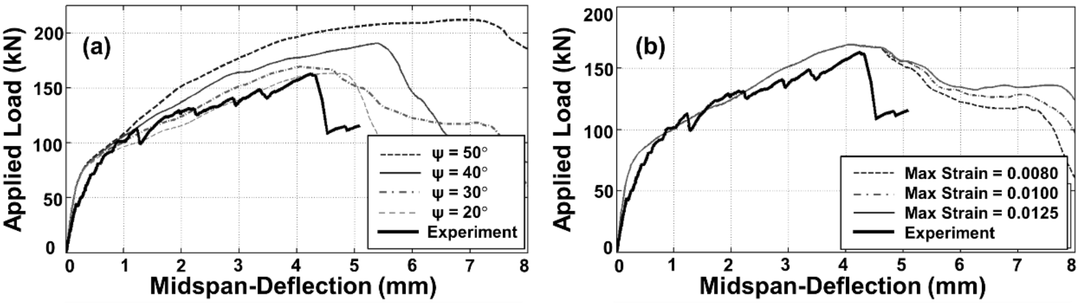

Fig. 12 BM12-INF. Influence of (a) Dilation angle ($\varepsilon_{c,max} = 0.008$), and (b) Maximum strain (ψ=30°)

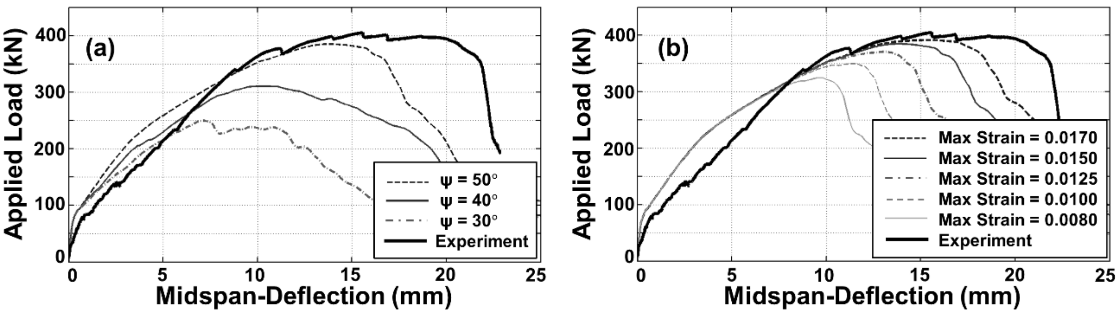

Fig. 13 BM 12-150. Influence of (a) Dilation angle ($\varepsilon_{c,max} = 0.015$), and (b) Maximum strain (ψ=50°)

Fig. 12(a) shows that as the dilation angle increases, the beam's response became more ductile and failed at higher loads with increased post peak stiffness and larger midspan deflections. It was concluded that a dilation angle of ψ = 30° consistently produced model responses that agreed strongest with the experimental beams without shear reinforcement. Furthermore, it was found that the response of beams without shear reinforcement is not dependent on the adopted maximum compressive strain (Fig. 12(b)).

For beams with shear reinforcement, the study first included analyses with different dilation angles ($\varepsilon_{c,max} = 0.015$), (Fig. 13(a)). The response is very dependent on the adopted value of the dilation angle. As the angle in increased, the model is able to produce a more ductile response of the confined (by stirrups) concrete which fails at higher loads and larger mid-span deflections. In Fig. 13(b) the dilation angle is constant (ψ=50°) and the maximum compressive strain varies. The response is highly dependent on the choice of $\varepsilon_{c,max}$. It was concluded that values of ψ=50° and $\varepsilon_{c,max} = 0.015$ provided results that consistently agreed strongest with the experimental data and were used in all further analyses of beams with shear reinforcement. It can be seen that the modelling of beams with GFRP shear reinforcement is much more sensitive to the selection of compression parameters than modelling of beams without shear reinforcement (compare Figs. 12 and 13). This introduces a unique challenge as compared to the modelling of concrete beams with plastic (yielding) steel stirrups where the failure is governed by stirrup yielding which is easier for a model to replicate.

5.3 Longitudinal reinforcement modelling

Linear truss elements and smeared membrane elements were used to model the longitudinal reinforcement. Fig. 14 compares the load-deflection responses for Beam 12-INF as produced by each method.

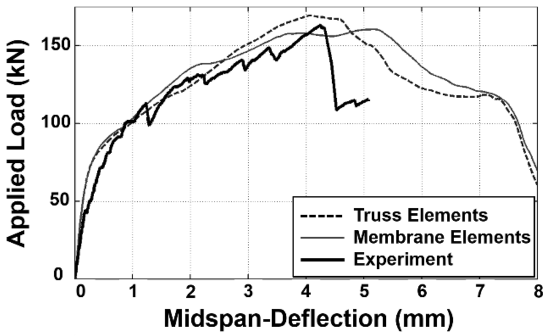

Fig. 14 Influence of reinforcement modelling method, Beam BM12-INF

Fig. 14 shows that both methods of modelling the reinforcement produced similar responses that agreed strongly with the experimental behaviour, both pre-peak and post-peak. The reinforcement axial strains produced by each modelling method were then compared to the data collected by the strain gauges used during the experimental testing. Fig. 15 presents the axial strains in the bottom layer of reinforcing bars at midspan for three beams without shear reinforcement.

Fig. 15 shows that the membrane strains match the truss elements' strains for each beam. This confirms that the membrane approach is capable of providing the same longitudinal stiffness properties as the discrete truss bars, and validates the use of embedded membranes to model reinforcement layers as an alternative to the traditional truss approach. However, the truss reinforcement method provided greater consistency across all models considered,

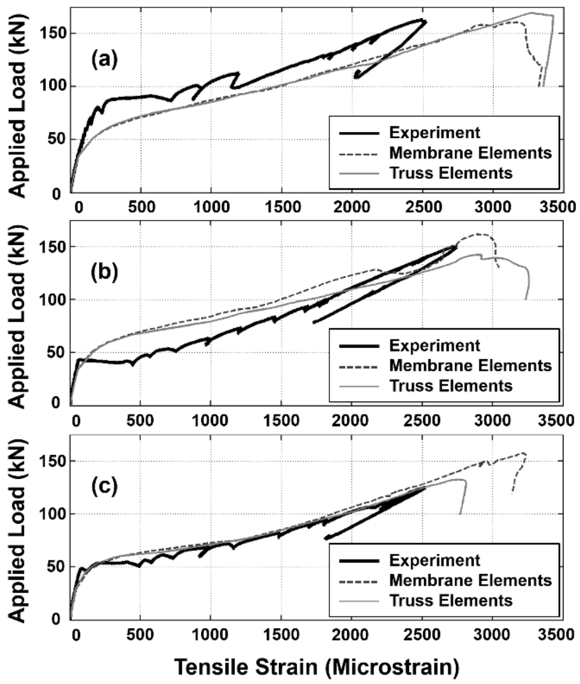

Fig. 15 Longitudinal reinforcement strains. (a) BM12-INF; (b) BM16-INF; (c) BM25-INF

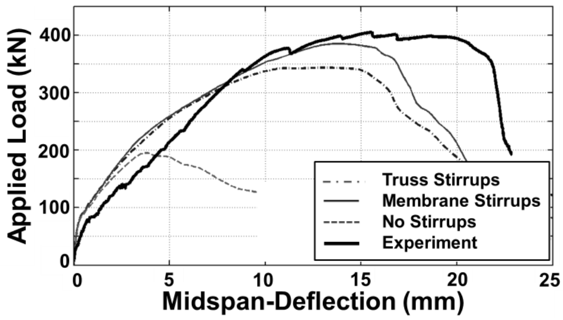

Fig. 16 Influence of Stirrups (ψ=50° & $\varepsilon_{c,max}$ =0.015) - BM 12-150

and allows for easier visualization of the stress distribution within each individual bar. Therefore, the truss approach was concluded to be the optimal method of modelling the longitudinal bars.

5.4 Modelling of stirrups

Fig. 16 presents the influence of the stirrup modelling method on the load-deflection response of BM 12-150 (ψ=50° and $\varepsilon_{c,max} = 0.015$). It can be seen that the use of membrane-section stirrups provided results that matched the experimental response closer than the truss element method. This can be investigated and explained further by reviewing the stirrup strains at three different locations (see Fig. 17). A consistent observation is that the truss-stirrup strains match closely with the membrane-stirrup strains initially. At failure, however, the truss-stirrups exhibited brittle responses, whereas the membrane-stirrups exhibited much higher ductility. It is clear that the use of membrane sections to model the stirrups allowed the stirrups to carry higher

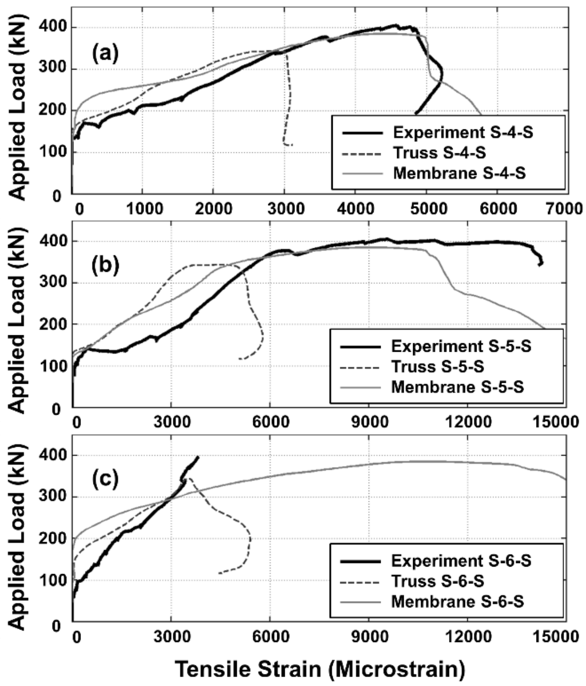

Fig. 17 Influence of stirrup modelling on strains - BM 12-150

tensile strains. This higher utilization of the stirrups resulted in the increased strength of these beams as compared to the truss-stirrup models. It is important to note that the strain gauge at S-6-S failed prior to the peak load during the experimental testing, which explains the sudden loss of data as shown in Fig. 17.

5.5 Finite element mesh

The influence of the concrete mesh density on the beams' responses was studied by considering five meshes, with each mesh characterized by the number of elements in the depth of the beam. The study was performed for beams without shear reinforcement and then the recommended mesh was used for beams with shear reinforcement. The coarsest mesh considered used 5 elements throughout the beam depth while the finest mesh used 21 elements. All alternatives used elements with aspect ratios of 1.0. Fig. 18(a) shows the influence of the mesh refinement on the load-deflection response for Beam 25-INF. Fig. 18(b) presents the plastic strain distribution at failure for each mesh alternative; these strains were used to visualize the concrete crack patterns. Note that Fig. 18(b) shows half of each beam, with the midspan located to the right.

Fig. 18(b) shows that all mesh densities accurately capture the presence of diagonal shear cracks propagating from the support towards the point of load application at midspan. As the mesh is refined, the crack pattern remains similar, but the crack bands become narrower and better defined. The use of finer meshes, 12-deep to 21-deep, provide crack patterns that match strongly with the experimentally observed crack pattern at failure. These results are consistent for all beams considered in this paper.

Fig. 18(a) shows that all mesh densities yielded failure

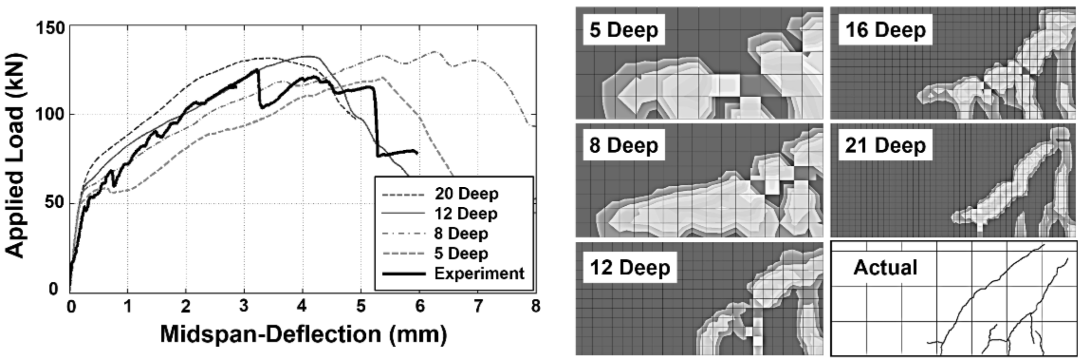

(a) (b)

Fig. 18 Influence of concrete mesh density, Beam 25-INF: (a) Load-deflection response; (b) Crack pattern at failure

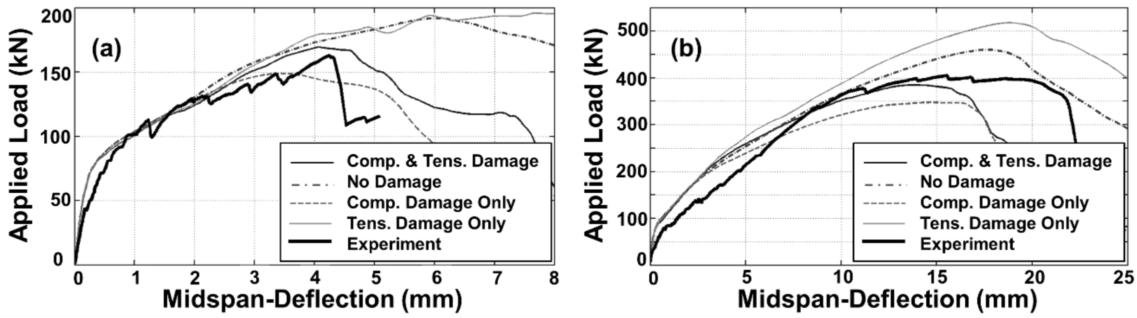

Fig. 19 Influence of damage: (a) BM 12-INF, (b) BM 12-150

loads that were within approximately 8% of the experimental peak load. The deflection responses, however, present an interesting pattern that was consistent for all beams. As the mesh became finer, the pre-failure deflection response became stiffer. This observation contradicts the typical behaviour of finite element models where a finer mesh provides less restraint to nodal displacements, thus yielding responses that are less stiff. Furthermore, it appears that the model does not converge to a final response with continued mesh refinement. DSS (2012) attributes this mesh sensitivity to regions of the concrete with little or no reinforcement. In these regions, cracking failures are not distributed evenly and may lead to localization of cracking. With mesh refinement, the crack bands will continue to become narrower and more localized, thus preventing the model from converging to a unique solution. Furthermore, the modelling of tension stiffening, and thus post-cracking stiffness, is dependent on the adopted fracture energy value and the size of the elements. Larger elements with larger characteristic lengths, l_c, will experience smaller tensile strains at a given fracture energy and will therefore experience less tension stiffening and a less stiff post-cracking response.

It was concluded that a mesh density with 12 elements in the depth of the beam was able to produce results that consistently agreed with the experimental data, while optimizing the computational efficiency of the models.

5.6 Damage modelling

The influence of incorporating damage into the beam models was studied. Fig. 19(a) shows the influence of incorporating damage parameters on the response for beam BM 12-INF, which was typical for all beams without shear reinforcement. The beam's response in the service loading region is similar regardless if damage is included or not. The beam that considered both compression and tension damage failed at a load very close to that of the experimental beam, whereas a larger peak load and higher degree of ductility are observed when damage is omitted. Note that the model response without damage was similar to the response with tension damage only; similarly, the response with both tension and compression damage was similar to the response with compression damage only. Therefore, tension damage modelling had little influence on the behaviour of beams with no stirrups since the beams failed shortly after cracking.

Fig. 19(b) shows the responses for beam BM 12-150, which was typical for all beams with stirrups, regardless of stirrup spacing or longitudinal bar arrangement. Similar to the beams with no stirrups, adding compression damage to the model significantly reduces the stiffness and strength of the beams. This shows that the stiffness degradation of concrete under compression plays a significant role in the structure's response, even under monotonic loading. Tension damage only, within the CDP model in ABAQUS, increases the strength and stiffness of the predicted response. Similar findings were noted by Genikomsou and Polak (2015) for concrete slabs failing in punching shear. After considering analyses of all beams, it was concluded that the use of both compression and tension damage parameters yields responses that match closest to the experimental data.

Table 4 Summary of recommended models

Model Parameter	Recommended Approach / Value	
	No Stirrups	With Stirrups
Compression Model:	Hognestad Parabola	Modified Hognestad Parabola
Maximum Compressive Strain:	N/A	0.015
Tension Model:	Bilinear Stress-Displacement Curve	Bilinear Stress-Displacement Curve
Fracture Energy, G_f:	90 N/m	90 N/m
Damage Parameters, d_c & d_t:	Tension and Compression Included	Tension and Compression Included
Dilation Angle, ψ:	30°	50°
σ_{bo}/σ_{co}:	1.16	1.16
Eccentricity, ϵ:	0.10	0.10
K_c:	2/3	2/3
Viscosity Parameter, μ:	0.0001	0.0001
Mesh Refinement:	12 Elements Deep	12 Elements Deep
Longitudinal Reinforcement:	Linear Truss Elements	Linear Truss Elements
Stirrup Reinforcement:	N/A	Reinforced Membrane Sections

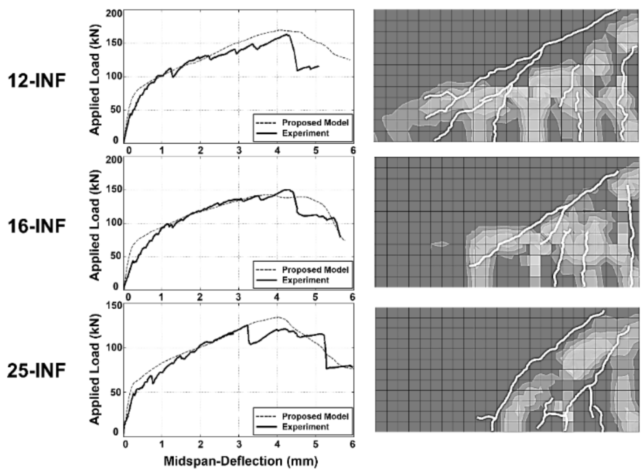

(a) (b)

Fig. 20 Proposed model results: (a) Load-deflection response; (b) Crack pattern at failure

6. Proposed models and results

Table 4 summarizes the recommended parameters for the effective modelling of concrete beams reinforced with or without GFRP stirrups and GFRP longitudinal bars using the Concrete Damaged Plasticity Model.

Figs. 20 to 23 present the applied load vs. midspan deflection responses for all beams studied in the paper. Also presented are the plastic strain distributions at failure for each beam as provided by the proposed model; these strains were used to visualize the crack patterns. The actual crack patterns at failure as observed during the experimental testing are superimposed in white. These results show that the proposed ABAQUS models are able to provide beam responses and crack patterns within acceptable accuracy.

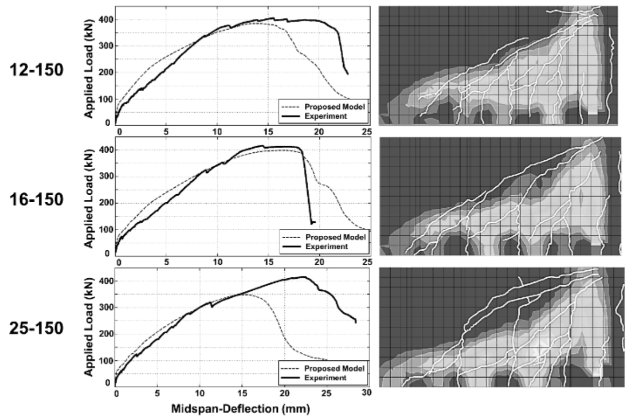

(a) (b)

Fig. 21 Proposed model results for BM XX-150: (a) Load-deflection response; (b) Crack pattern at failure

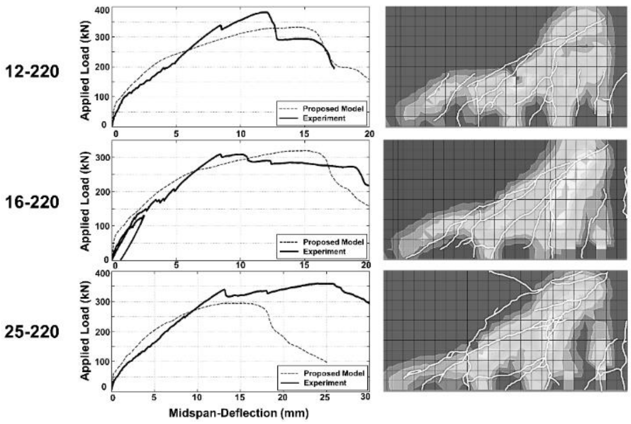

(a) (b)

Fig. 22 Proposed model results for BM XX-220: (a) Load-deflection response; (b) Crack pattern at failure

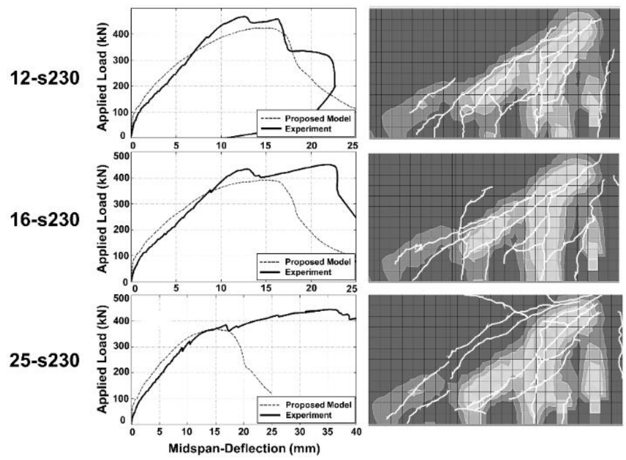

(a) (b)

Fig. 23 Proposed model results for BM XX-s230: (a) Load-deflection response; (b) Crack pattern at failure

7. Comparison to strength prediction models

The failure loads predicted by the proposed analytical models were compared to three strength prediction models,

Table 5 Comparison of predicted and experimental failure loads

Beam	Exper.	CSA S806-12 Flexure		CSA S806-12 Shear		Nehdi *et al*. Shear		ABAQUS Model	
	P_E (kN)	P_P (kN)	Ratio P_E/P_P	P_P (kN)	Ratio P_E/P_P	P_P (kN)	Ratio P_E/P_P	P_P (kN)	Ratio P_E/P_P
12-INF	163.1	431.9	0.38	152.8	1.07	151.3	1.08	169.4	0.96
16-INF	150.2	410.3	0.37	144.8	1.04	146.9	1.02	142.3	1.06
25-INF	125.1	372.5	0.34	131.8	0.95	139.3	0.90	132.5	0.94
12-150	405.2	441.9	0.92	226.2	1.79	376.7	1.08	385.1	1.05
16-150	416.5	422.0	0.99	214.4	1.94	372.7	1.12	398.6	1.04
25-150	415.8	388.0	1.07	195.4	2.13	365.7	1.14	348.6	1.19
12-220	382.4	441.9	0.87	206.2	1.85	337.0	1.13	332.2	1.15
16-220	309.3	422.0	0.73	195.7	1.58	333.0	0.93	319.7	0.97
25-220	360.1	388.0	0.93	178.9	2.01	326.0	1.10	294.1	1.22
12-s230	466.9	484.0	0.96	293.3	1.59	477.9	0.98	422.5	1.11
16-s230	434.0	462.0	0.94	277.0	1.57	473.4	0.92	391.8	1.11
25-s230	388.7	424.0	0.92	245.5	1.58	465.7	0.83	368.1	1.06

including: (a) flexural strength predicted by CSA S806-12, (b) shear strength predicted by CSA S806-12, and (c) shear strength predicted by Nehdi *et al*. (2007).

The shear models proposed by CSA S806 and Nehdi *et al*. (2007) both calculate the shear resistance of an FRP reinforced concrete section by summing the contribution of the concrete with the contribution of the shear reinforcement (stirrups). A detailed description of these models is presented in Stoner (2015). Herein, Table 5 compares the failure loads as provided by the experimental tests (P_E) to the failure loads provided by the proposed FEA models and strength prediction models (P_P).

The flexural strengths predicted by CSA S806 for beams without shear reinforcement significantly overestimate the failure loads as compared to the experimental failure loads; this is to be expected as all beams experienced shear failures. The shear strengths predicted by CSA S806 and Nehdi *et al*. (2007) were able to predict the failure loads to within 6.3% and 11.4% of the experimental peak loads, respectively. The proposed ABAQUS model was able to accurately predict the failure load to within 6.0% of the experimental values for the beams without shear reinforcement.

The shear strength predictions of CSA S806-12 severely underestimated the shear strength of all beams with shear reinforcement and provided the weakest correlation with the ABAQUS and experiment results. The shear strength predictions proposed by Nehdi *et al*. (2007) provided the best agreement to the ABAQUS results for beams with stirrups spaced at 150mm and 220mm. The CSA S806-12 flexure formulas provided better results for beams with stirrups spaced at 230mm than the shear formulas; however, these beams failed due to shear and thus this result suggests that further improvements to the design provisions are necessary.

8. Conclusions

This paper presents a methodology for the effective modelling of concrete beams reinforced with GFRP longitudinal and transverse bars using the Concrete Damaged Plasticity Model within ABAQUS. Several aspects of modelling are discussed in the paper, namely, concrete modelling, concrete confinement, cracking, and meshing. The model was calibrated using experimental reference tests and, once calibrated, the proposed model was able to accurately predict failure loads, deflection responses, crack patterns, and reinforcement strains that matched the experimental results. It was shown that the current design provisions of CSA S806-12 require further development; the design of GFRP members must be based on studying load transfer mechanisms in concrete reinforced with linear elastic brittle reinforcements, which are different than those mechanisms for concrete reinforced with linear elastic plastic (e.g., steel) reinforcements. The proposed methodology can be successfully applied for parametric studies on the behaviour of concrete beams reinforced with linear elastic brittle reinforcements (e.g., GFRP bars) and for further development of design recommendations for such members.

Acknowledgements

The authors would like to thank the Ontario Centres of Excellence, Natural Sciences and Engineering Research Council of Canada, and Schoeck Canada for their financial contributions to this research.

References

Adam, M.A., Said, M., Mahmoud, A.A. and Shanour, A.S. (2015), "Analytical and experimental flexural behavior of concrete beams reinforced with glass fiber reinforced polymers bars", *Constr. Build. Mater.*, **84**, 354-366. https://doi.org/10.1016/j.conbuildmat.2015.03.057.

Arafa, A., Farghaly, A.S. and Benmokrane, B., (2019), "Nonlinear finite-element analysis for predicting the behavior of concrete squat walls reinforced with GFRP bars", *J. Struct. Eng.*, ASCE, **145**(10), 04019107. https://doi.org/10.1061/(ASCE)ST.1943-541X.0002399.

Canadian Standards Association (CSA). (2012), Design and Construction of Building Structures with Fibre-Reinforced Polymers, CAN/CSA S806-12, Mississauga, Ontario.

CEB-FIP (1993), Model Code 1990 (MC 90), Design Code, Thomas Telford, London.

Cornelissen, H., Hordijk, D. and Reinhardt, H. (1986), "Experimental determination of crack softening characteristics of normal weight and lightweight concrete", *Heron*, **32**(2), 45-56.

Dassault Systems Simulia Corp. (DSS) (2012), ABAQUS Analysis User's Manual 6.12, Providence, RI, USA.

Ferreira, A.J.M., Camanho, P.P., Marques, A.T. and Fernandes, A.A. (2001), "Modelling of concrete beams reinforced with FRP re-bars", *Compos. Struct.*, **53**(1), 101-116. https://doi.org/10.1016/S0263-8223(00)00182-3.

Genikomsou, A. and Polak, M.A. (2015), "Finite element analysis of punching shear of concrete slabs using damaged plasticity model in Abaqus", *Eng. Struct.*, **98**(4), 38-48. https://doi.org/10.1016/j.engstruct.2015.04.016.

Hillerborg, A., Modeer, M. and Petersson, P. (1976), "Analysis of crack formation and crack growth in concrete by means of fracture mechanics and finite elements", *Cement Concrete Res.*, **6**(6), 773-782. https://doi.org/10.1016/0008-8846(76)90007-7.

International Federation for Structural Concrete (2008), Constitutive Modelling of High Strength/High Performance Concrete - Bulletin 42, Lausanne, Switzerland.

International Federation for Structural Concrete (2010), Model Code 2010. First Complete Draft, Version 1, Lausanne, Switzerland.

International Federation for Structural Concrete (2013), Code-Type Models for Structural Behaviour of Concrete, Lausanne, Switzerland.

Jankowiak, T. and Lodygowski, T. (2005), "Identification of parameters of concrete damage plasticity constitutive model". *Found. Civil Environ. Eng.*, **6**(1), 53-69.

Jumaaa, G.B. and Yousif, A.R. (2019), "Numerical modeling of size effect in shear strength of FRP-reinforced concrete beams", *Struct.*, **20**, 237-254. https://doi.org/10.1016/j.istruc.2019.04.008.

Kaya, M. and Yaman, C. (2018), "Modelling the reinforced concrete beams strengthened with GFRP against shear crack", *Comput. Concrete*, **21**(2), 127-137. https://doi.org/10.12989/cac.2018.21.2.127.

Krall, M. (2014), "Tests on concrete beams with GFRP flexural and shear reinforcements & analysis method for indeterminate strut-and-tie models with brittle reinforcements", Master's Thesis, University of Waterloo, Canada.

Kupfer, H., Hilsdorf, H. and Rusch, H. (1969), "Behaviour of concrete under biaxial stresses", *ACI J. Proc.*, **66**(8), 656-666.

Lee, J. and Fenves, G. (1998), "Plastic-damage model for cyclic loading of concrete structures", *J. Eng. Mech.*, **124**(8), 892-900. https://doi.org/10.1061/(ASCE)0733-9399(1998)124:8(892).

Lubliner, J., Oliver, J., Oller, S. and Onate, E. (1989), "A plastic-damage model for concrete", *Int. J. Solid. Struct.*, **25**(3), 299-326. https://doi.org/10.1016/0020-7683(89)90050-4.

Malm, R. (2006), "Shear cracks in concrete structures subjected to in-plane stresses", Thesis, Royal Institute of Technology, Stockholm, Sweden.

Mohamed, K., Farghaly, A.S., Benmokrane, B. and Neale, K.W. (2017), "Nonlinear finite-element analysis for the behavior prediction and strut efficiency factor of GFRP-reinforced concrete deep beams", *Eng. Struct.*, **137**, 145-161. https://doi.org/10.1016/j.engstruct.2017.01.045.

Nehdi, M., Chabib, H.E. and Said, A.A. (2007), "Proposed shear design equations for FRP-reinforced concrete beams based on genetic algorithms approach", *J. Mater. Civil Eng.*, **19**(12), 1033-1042. https://doi.org/10.1061/(ASCE)0899-1561(2007)19:12(1033).

Nour, A., Massicotte, B., Yildiz, E. and Koval, V. (2007), "Finite element modelling of concrete structures reinforced with internal and external fibre-reinforced polymers", *Can. J. Civil Eng.*, **34**(3), 340-354. https://doi.org/10.1139/l06-140.

Petersson, P. (1981), "Crack growth and development of fracture zones in plain concrete and similar materials", Report TVBM - 1006, Lund Institute of Technology, Lund, Sweden.

Polling, R. (2001), "Eine Praxisnahe, Schdigungsorientierte Materialbeschreibung von Stahlbeton", Dissertation, Ruhr-Universitt Bochum, Germany.

Rafi, M.M., Nadjai, A. and Ali, F. (2007), "Analytical modeling of concrete beams reinforced with carbon FRP bars", *J. Compos. Mater.*, **41**(22), 2675-2690. https://doi.org/10.1177/0021998307078728.

Reineck, K., Kuchma, D., Kim, K. and Marx, S. (2003), "Shear data for reinforced concrete members with shear reinforcement", *ACI Struct. J.*, **100**(2), 240-249.

Saleh, Z., Sheikh, M.N., Remennikow, A. and Basu, A. (2019), "Numerical analysis of behavior of glass fiber-reinforced polymer bar-reinforced concrete beams under impact loads", *ACI Struct. J.*, **116**(5), 151-160.

Stoner, J. (2015), "Finite element modelling of GFRP reinforced concrete beams", Master's Thesis, University of Waterloo, Canada.

Trunk, B. and Wittmann, F. (1998), "Experimental investigation into the size dependence of fracture mechanics parameters", *Third International Conference of Fracture Mechanics of Concrete Structures*, **3**, 1937-1948.

Yu, T., Teng, J., Wong, Y. and Dong, S. (2010), "Finite element modeling of confined concrete-I: Drucker Prager type plasticity model", *Eng. Struct.*, **32**(3), 665-679. https://doi.org/10.1016/j.engstruct.2009.11.014

SF